Performance of Rake Receivers in IR-UWB Networks Using Energy-Efficient Power Control

Giacomo Bacci, Marco Luise and H. Vincent Poor

Abstract

This paper studies the performance of partial-Rake (PRake) receivers in impulse-radio ultrawideband wireless networks when an energy-efficient power control scheme is adopted. Due to the large bandwidth of the system, the multipath channel is assumed to be frequency-selective. By making use of noncooperative game-theoretic models and large-system analysis tools, explicit expressions are derived in terms of network parameters to measure the effects of self-interference and multiple-access interference at a receiving access point. Performance of the PRake receivers is thus compared in terms of achieved utilities and loss to that of the all-Rake receiver. Simulation results are provided to validate the analysis.

Index Terms

Energy-efficiency, impulse-radio, ultrawideband systems, Rake receivers, large-system analysis.

I. INTRODUCTION

Ultrawideband (UWB) technology is considered to be a potential candidate for next-generation multiuser data networks, due to its large spreading factor (which implies large multiuser capacity) and its lower spectral density (which allows coexistence with incumbent systems in the same frequency bands). The requirements for designing high-speed wireless data terminals include efficient resource allocation and interference reduction. These issues aim to allow each user to achieve the require quality of service (QoS) at the uplink receiver without causing unnecessary interference to other users in the system, and minimizing power consumption. Energy-efficient power control techniques can be derived making use of

G. Bacci and M. Luise are with the Dipartimento Ingegneria dell'Informazione, Università di Pisa, Pisa, 56122 Italy (e-mail: giacomo.bacci@iet.unipi.it, marco.luise@iet.unipi.it).

H. V. Poor is with the Department of Electrical Engineering, Princeton University, Princeton, NJ 08544 USA (e-mail: poor@princeton.edu).

game theory [1]–[6]. In [1], the authors provide motivations for using game theory to study power control in communication systems and ad-hoc networks. In [2], power control is modeled as a noncooperative game in which the users choose their transmit powers to maximize their utilities, defined as the ratio of throughput to transmit power. In [3], [4], the authors use pricing to obtain a more efficient solution for the power control game, while the cross-layer problem of joint multiuser detection and power control is studied in [5]. A game-theoretic approach for a UWB system is studied in [6], where the channel fading is assumed to be frequency-selective, due to the large bandwidth occupancy [7]–[9].

This work extends the results of [6], where a theoretical method to analyze transmit powers and utilities achieved in the uplink of an infrastructure network at the Nash equilibrium has been proposed. However, explicit expressions have been derived in [6] only for all-Rake (ARake) receivers [10] at the access point, under the assumption of a flat averaged power delay profile (aPDP) [11]. This paper considers partial-Rake (PRake) receivers at the access point and makes milder hypotheses on the channel model. Resorting to a large-system analysis, we obtain a general characterization of the effects of multiple access interference (MAI) and self-interference (SI), which allows explicit expressions for the utilities achieved at the Nash equilibrium to be derived. Furthermore, we obtain an approximation to the loss of the PRake receivers with respect to (wrt) the ARake receivers in terms of energy-efficiency, which involves only network parameters and receiver characteristics. Since this loss is independent of the channel realizations, it can serve as a network design criterion.

The remainder of the paper is organized as follows. Some background for this work is given in Sect. II, where the system model is described (Sect. II-A) and the results of the game-theoretic power control approach are shown (Sect. II-B). In Sect. III, we use a large-system analysis to evaluate the effects of the interference at the Nash equilibrium. Results are shown for the general case, as well as for some particular scenarios (including the one proposed in [6]). Performance of the PRake receivers at the Nash equilibrium is analyzed in Sect. IV, where also a comparison with simulation results is provided. Some conclusions are drawn in Sect. V.

II. BACKGROUND

A. System Model

Commonly, impulse-radio (IR) systems, which transmit very short pulses with a low duty cycle, are employed to implement UWB systems [12]. We focus on a binary phase shift keying (BPSK) time hopping (TH) IR-UWB system with polarity randomization [13]. A network with K users transmitting to a receiver at a common concentration point is considered. The processing gain of the system is assumed

to be $N = N_f \cdot N_c$, where N_f is the number of pulses that represent one information symbol, and N_c denotes the number of possible pulse positions in a frame [12]. The transmission is assumed to be over *frequency selective channels*, with the channel for user k modeled as a tapped delay line:

$$c_k(t) = \sum_{l=1}^{L} \alpha_l^{(k)} \delta(t - (l-1)T_c - \tau_k), \tag{1}$$

where T_c is the duration of the transmitted UWB pulse, which is the minimum resolvable path interval; L is the number of channel paths; $\boldsymbol{\alpha}_k = [\alpha_1^{(k)}, \ldots, \alpha_L^{(k)}]^T$ and τ_k are the fading coefficients and the delay of user k, respectively. Considering a chip-synchronous scenario, the symbols are misaligned by an integer multiple of the chip interval T_c: $\tau_k = \Delta_k T_c$, for every k, where Δ_k is uniformly distributed in $\{0, 1, \ldots, N-1\}$. In addition we assume that the channel characteristics remain unchanged over a number of symbol intervals. This can be justified since the symbol duration in a typical application is on the order of tens or hundreds of nanoseconds, and the coherence time of an indoor wireless channel is on the order of tens of milliseconds.

Due to high resolution of UWB signals, multipath channels can have hundreds of multipath components, especially in indoor environments. To mitigate the effect of multipath fading as much as possible, we consider an access point where K Rake receivers [10] are used.[1] The Rake receiver for user k is in general composed of L coefficients, where the vector $\boldsymbol{\beta}_k = \mathbf{G} \cdot \boldsymbol{\alpha}_k = [\beta_1^{(k)}, \ldots, \beta_L^{(k)}]^T$ represents the combining weights for user k, and the $L \times L$ matrix $\mathbf{G}$ depends on the type of Rake receiver employed. In particular, if $\mathbf{G}$ is a deterministic diagonal matrix, with

$$\{\mathbf{G}\}_{ll} = \begin{cases} 1, & 1 \le l \le r \cdot L, \\ 0, & \text{elsewhere,} \end{cases} \tag{2}$$

where $r \triangleq L_P/L$ and $0 < L_P \le L$, a PRake with L_P fingers using maximal ratio combining (MRC) is considered. It is worth noting that, when $r = 1$, an ARake is implemented.

The signal-to-interference-plus-noise ratio (SINR) of the kth user at the output of the Rake receiver can be well approximated[2] by [14]

$$\gamma_k = \frac{h_k^{(SP)} p_k}{h_k^{(SI)} p_k + \sum_{\substack{j=1 \\ j \ne k}}^{K} h_{kj}^{(MAI)} p_j + \sigma^2}, \tag{3}$$

[1]Since the focus of this work is on the interplay between power control and Rake receivers, perfect channel estimation is considered throughout the paper for ease of calculation.

[2]This approximation is valid for large N_f (typically, at least 5).

where σ^2 is the variance of the additive white Gaussian noise (AWGN) at the receiver, and the gains are expressed by

$$h_k^{(\text{SP})} = \boldsymbol{\beta}_k^H \cdot \boldsymbol{\alpha}_k, \tag{4}$$

$$h_k^{(\text{SI})} = \frac{1}{N} \frac{\left|\left| \boldsymbol{\Phi} \cdot \left(\mathbf{B}_k^H \cdot \boldsymbol{\alpha}_k + \mathbf{A}_k^H \cdot \boldsymbol{\beta}_k \right) \right|\right|^2}{\boldsymbol{\beta}_k^H \cdot \boldsymbol{\alpha}_k}, \tag{5}$$

and

$$h_{kj}^{(\text{MAI})} = \frac{1}{N} \frac{\left|\left| \mathbf{B}_k^H \cdot \boldsymbol{\alpha}_j \right|\right|^2 + \left|\left| \mathbf{A}_j^H \cdot \boldsymbol{\beta}_k \right|\right|^2 + \left| \boldsymbol{\beta}_k^H \cdot \boldsymbol{\alpha}_j \right|^2}{\boldsymbol{\beta}_k^H \cdot \boldsymbol{\alpha}_k}, \tag{6}$$

where

$$\mathbf{A}_k = \begin{pmatrix} \alpha_L^{(k)} & \cdots & \cdots & \alpha_2^{(k)} \\ 0 & \alpha_L^{(k)} & \cdots & \alpha_3^{(k)} \\ \vdots & \ddots & \ddots & \vdots \\ 0 & \cdots & 0 & \alpha_L^{(k)} \\ 0 & \cdots & \cdots & 0 \end{pmatrix}, \tag{7}$$

$$\mathbf{B}_k = \begin{pmatrix} \beta_L^{(k)} & \cdots & \cdots & \beta_2^{(k)} \\ 0 & \beta_L^{(k)} & \cdots & \beta_3^{(k)} \\ \vdots & \ddots & \ddots & \vdots \\ 0 & \cdots & 0 & \beta_L^{(k)} \\ 0 & \cdots & \cdots & 0 \end{pmatrix}, \tag{8}$$

$$\boldsymbol{\Phi} = \text{diag} \left\{ \phi_1, \ldots, \phi_{L-1} \right\}, \tag{9}$$

and

$$\phi_l = \sqrt{\frac{\min\{L - l, N_c\}}{N_c}} \tag{10}$$

have been introduced for convenience of notation.

B. The Game-Theoretic Power Control Game

Consider the application of noncooperative power control techniques to the wireless network described above. Focusing on mobile terminals, where it is often more important to maximize the number of bits transmitted per Joule of energy consumed than to maximize throughput, an energy-efficient approach like the one described in [6] is considered.

Game theory [1] is the natural framework for modeling and studying these interactions between users. It is thus possible to consider a noncooperative power control game in which each user seeks to maximize its own utility function as follows. Let $G = [\mathcal{K}, \{P_k\}, \{u_k(\mathbf{p})\}]$ be the proposed noncooperative game where $\mathcal{K} = \{1, \ldots, K\}$ is the index set for the users; $P_k = [\underline{p}_k, \overline{p}_k]$ is the strategy set, with $\underline{p}_k$ and $\overline{p}_k$ denoting minimum and maximum power constraints, respectively; and $u_k(\mathbf{p})$ is the payoff function for user k [4], defined as

$$u_k(\mathbf{p}) = \frac{D}{M} R_k \frac{f(\gamma_k)}{p_k}, \tag{11}$$

where $\mathbf{p} = [p_1, \ldots, p_K]$ is the vector of transmit powers; D and M are the number of information bits per packet and the total number of bits per packet, respectively; R_k and γ_k are the transmission rate and the SINR (3) for the kth user, respectively; and $f(\gamma_k)$ is the efficiency function representing the packet success rate (PSR), i.e., the probability that a packet is received without an error. Throughout this analysis, we assume $\underline{p}_k = 0$ and $\overline{p}_k = \overline{p}$ for all $k \in \mathcal{K}$.

Provided that the efficiency function is increasing, S-shaped, and continuously differentiable, with $f(0) = 0$, $f(+\infty) = 1$, and $f'(0) = df(\gamma_k)/d\gamma_k|_{\gamma_k=0} = 0$, it has been shown [6] that the solution of the maximization problem $\max_{p_k \in P_k} u_k(\mathbf{p})$ for $k = 1, \ldots, K$ is

$$p_k^* = \min\left\{ \frac{\gamma_k^* \left(\sum_{j \neq k} h_{kj}^{(\text{MAI})} p_j + \sigma^2 \right)}{h_k^{(\text{SP})} (1 - \gamma_k^*/\gamma_{0,k})}, \overline{p} \right\}, \tag{12}$$

where

$$\gamma_{0,k} = \frac{h_k^{(\text{SP})}}{h_k^{(\text{SI})}} = N \cdot \frac{(\boldsymbol{\beta}_k^H \cdot \boldsymbol{\alpha}_k)^2}{||\boldsymbol{\Phi} \cdot (\mathbf{B}_k^H \cdot \boldsymbol{\alpha}_k + \mathbf{A}_k^H \cdot \boldsymbol{\beta}_k)||^2} \geq 1 \tag{13}$$

and γ_k^* is the solution of

$$f'(\gamma_k^*)\gamma_k^* (1 - \gamma_k^*/\gamma_{0,k}) = f(\gamma_k^*), \tag{14}$$

where $f'(\gamma_k^*) = df(\gamma_k)/d\gamma_k|_{\gamma_k=\gamma_k^*}$. Since γ_k^* depends only on $\gamma_{0,k}$, for convenience of notation a function $\Gamma(\cdot)$ is defined such that $\gamma_k^* = \Gamma(\gamma_{0,k})$. Fig. 1 shows the shape of $\gamma_k^* = \Gamma(\gamma_{0,k})$, where the efficiency function is taken to be $f(\gamma_k) = (1 - e^{-\gamma_k/2})^M$, with $M = 100$.

Assuming the typical case of multiuser UWB systems, where $N \gg K$, and also considering $\overline{p}$ sufficiently large, (12) can be reduced to [6]

$$p_k^* = \frac{1}{h_k^{(\text{SP})}} \cdot \frac{\sigma^2 \Gamma(\gamma_{0,k})}{1 - \Gamma(\gamma_{0,k}) \cdot (\gamma_{0,k}^{-1} + \zeta_k^{-1})}, \tag{15}$$

where $\zeta_k^{-1} = \sum_{j \neq k} h_{kj}^{(\text{MAI})}/h_j^{(\text{SP})}$; and $\gamma_{0,k}^{-1}$ is defined as in (13).

A necessary and sufficient condition for the Nash equilibrium to be achieved simultaneously by all K users, and thus for (15) to be valid, is [6]

$$\Gamma\left(\gamma_{0,k}\right) \cdot \left(\gamma_{0,k}^{-1} + \zeta_k^{-1}\right) < 1 \quad \forall k \in \mathcal{K}. \tag{16}$$

As can be verified, the amount of transmit power p_k^* required to achieve the target SINR γ_k^* will depend not only on the gain $h_k^{(\text{SP})}$, but also on the SI term $h_k^{(\text{SI})}$ (through $\gamma_{0,k}$) and the interferers $h_{kj}^{(\text{MAI})}$ (through ζ_k).

III. ANALYSIS OF THE INTERFERENCE

In order to derive some quantitative results for the achieved utilities and for the transmit powers independent of SI and MAI terms, it is possible to resort to a large-system analysis.

Theorem 1 ([6]): Assume that $\alpha_k^{(l)}$ are zero-mean random variables independent across k and l, and $\mathbf{G}$ is a deterministic diagonal matrix (thus implying that $\alpha_k^{(l)}$ and $\beta_j^{(m)}$ are dependent only when $j = k$ and $m = l$). In the asymptotic case where K and N_f are finite,[3] while $L, N_c \to \infty$, with the ratio N_c/L approaching a constant, the terms ζ_k^{-1} and $\gamma_{0,k}^{-1}$ converge almost surely (a.s.) to

$$\zeta_k^{-1} \overset{a.s.}{\to} \frac{1}{N} \sum_{\substack{j=1 \\ j \neq k}}^{K} \frac{\varphi\left(\mathbf{D}_j^\alpha \mathbf{C}_k^\beta \mathbf{C}_k^{\beta H} \mathbf{D}_j^\alpha\right) + \varphi\left(\mathbf{D}_k^\beta \mathbf{C}_j^\alpha \mathbf{C}_j^{\alpha H} \mathbf{D}_k^\beta\right)}{\varphi\left(\mathbf{D}_j^\alpha \mathbf{D}_j^\beta\right) \cdot \varphi\left(\mathbf{D}_k^\alpha \mathbf{D}_k^\beta\right)} \tag{17}$$

and

$$\gamma_{0,k}^{-1} \overset{a.s.}{\to} \frac{1}{N} \frac{\lim\limits_{L \to \infty} \frac{1}{L^2} \sum\limits_{i=1}^{L-1} \phi_i^2 \cdot \sum\limits_{l=1}^{i} \theta_k^2\left(l, L+l-i\right)}{\left(\varphi\left(\mathbf{D}_k^\alpha \mathbf{D}_k^\beta\right)\right)^2}, \tag{18}$$

where ϕ_i is defined as in (10); $\mathbf{D}_j^\alpha$ and $\mathbf{D}_k^\beta$ are diagonal matrices whose elements are

$$\{\mathbf{D}_j^\alpha\}_l = \sqrt{\mathbb{V}\text{ar}[\alpha_j^{(l)}]}, \tag{19}$$

and

$$\{\mathbf{D}_k^\beta\}_l = \sqrt{\mathbb{V}\text{ar}[\beta_k^{(l)}]}, \tag{20}$$

[3]In order for the analysis to be consistent, and also considering regulations by the US Federal Communications Commission (FCC) [15], it is worth noting that N_f could not be smaller than a certain threshold ($N_f \geq 5$).

with $\mathbb{Var}[\cdot]$ denoting the variance of a random variable; $\mathbf{C}_j^\alpha$ and $\mathbf{C}_j^\beta$ are $L \times (L-1)$ matrices whose elements are

$$\{\mathbf{C}_j^\alpha\}_{li} = \sqrt{\frac{\mathbb{Var}[\{\mathbf{A}_j\}_{li}]}{L}}, \tag{21}$$

and

$$\{\mathbf{C}_k^\beta\}_{li} = \sqrt{\frac{\mathbb{Var}[\{\mathbf{B}_k\}_{li}]}{L}}; \tag{22}$$

$\varphi(\cdot)$ is the matrix operator

$$\varphi(\cdot) = \lim_{L\to\infty} \frac{1}{L} \mathrm{Tr}(\cdot), \tag{23}$$

with $\mathrm{Tr}(\cdot)$ denoting the trace operator; and

$$\theta_k(l, L+l-i) = \{\mathbf{D}_k^\alpha\}_l\{\mathbf{D}_k^\beta\}_{L+l-i} + \{\mathbf{D}_k^\beta\}_l\{\mathbf{D}_k^\alpha\}_{L+l-i}. \tag{24}$$

The proof of this theorem can be found in [6].

The results above can be applied to any kind of fading model, as long as the second-order statistics are available. Furthermore, due to the symmetry of (17) and (18), it is easy to verify that the results are independent of large-scale fading models. Hence, Theorem 1 applies to any kind of channel, which may include both large- and small-scale statistics.

Channel modeling for IR-UWB systems is still an open issue. In fact, while there exists a commonly agreed-on set of basic models for narrowband and wideband wireless channels [16], a similarly well accepted UWB channel model does not seem to exist. Recently, two models, namely IEEE 802.15.3a [8] and IEEE 802.15.4a [9], have been standardized to properly characterize the UWB environment. However, for ease of calculation, the expressions derived in the remainder of the paper consider the following simplifying assumptions:

- The channel gains are independent complex Gaussian random variables with zero means and variances $\sigma_{k_l}^2$, i.e., $\alpha_k^{(l)} \sim \mathcal{CN}(0, \sigma_{k_l}^2)$. This assumption leads $|\alpha_k^{(l)}|$ to be Rayleigh-distributed with parameter $\sigma_{k_l}^2/2$. Although both IEEE 802.15.3a and IEEE 802.15.4a models include some forms of Nakagami m distribution for the channel gains, the Rayleigh distribution, appealing for its analytical tractability, has recently been shown [17] to provide a good approximation for multipath propagation in UWB systems.

- Lately, a clustering phenomenon for the aPDP [11] in IR-UWB multipath channels has emerged from a large number of UWB measurement campaigns [18], [19]. However, owing to the analytical difficulties arising when considering such aspect, this work focuses on an exponentially decaying

aPDP, as is customarily used in several UWB channel models [20], [21]. This translates into the hypothesis

$$\sigma_{k_l}^2 = \sigma_k^2 \cdot \Lambda^{-\frac{l-1}{L-1}}, \tag{25}$$

where

$$\Lambda = \sigma_{k_1}^2 / \sigma_{k_L}^2 \tag{26}$$

and the variance σ_k^2 depends on the distance between user k and the access point. Fig. 2 shows the aPDP for some values of Λ versus the normalized excess delay, i.e., the ratio between the excess delay, lT_c, and the maximum excess delay considered, LT_c. It is easy to verify that $\Lambda = 0\,\mathrm{dB}$ represents the case of flat aPDP.

Using these hypotheses, the matrices $\mathbf{D}_k^\alpha$ and $\mathbf{D}_k^\beta$ can be expressed in terms of

$$\{\mathbf{D}_k^\alpha\}_l = \sigma_k \cdot \Lambda^{-\frac{l-1}{2(L-1)}} \cdot u\,[L-l] \tag{27}$$

and

$$\{\mathbf{D}_k^\beta\}_l = \sigma_k \cdot \Lambda^{-\frac{l-1}{2(L-1)}} \cdot u\,[r \cdot L - l], \tag{28}$$

where

$$u\,[n] = \begin{cases} 1, & n \geq 0, \\ 0, & n < 0. \end{cases} \tag{29}$$

A. PRake with exponentially decaying aPDP

Prop. 1: In the asymptotic case where the hypotheses of Theorem 1 hold, when adopting a PRake with L_P coefficients according to the MRC scheme,

$$\zeta_k^{-1} \overset{a.s.}{\to} \frac{K-1}{N} \cdot \mu\,(\Lambda, r), \tag{30}$$

where

$$\mu\,(\Lambda, r) = \frac{(\Lambda - 1) \cdot \Lambda^{r-1}}{\Lambda^r - 1}, \tag{31}$$

and $r \triangleq L_P/L$, $0 < r \leq 1$.

The proof can be found in App. A.

Prop. 2: In the asymptotic case where the hypotheses of Theorem 1 hold, when adopting a PRake with L_P coefficients according to the MRC scheme,

$$\gamma_{0,k}^{-1} \overset{a.s.}{\to} \frac{1}{N} \cdot \nu\left(\Lambda, r, \rho\right), \tag{32}$$

where $\rho \triangleq N_c/L$, $0 < \rho < \infty$, $r \triangleq L_P/L$, $0 < r \leq 1$, and

$$\nu\left(\Lambda, r, \rho\right) = \begin{cases} \frac{\Lambda(\Lambda^\rho-1)\left(4\Lambda^{2r}+3\Lambda^\rho-1\right)-2\Lambda^{r+\rho}(\Lambda^r+3\Lambda-1)\rho\log\Lambda}{2(\Lambda^r-1)^2\rho\Lambda^{1+\rho}\log\Lambda}, \\ \qquad \text{if } 0 \leq \rho \leq \min(r, 1-r); & (33a) \\[2mm] \frac{\Lambda(4\Lambda^\rho-1)\left(\Lambda^{2r}-1\right)-2\Lambda^{r+\rho}(3\Lambda r-\rho+\Lambda^r\rho)\log\Lambda}{2(\Lambda^r-1)^2\rho\Lambda^{1+\rho}\log\Lambda}, \\ \qquad \text{if } \min(r, 1-r) \leq \rho \leq \max(r, 1-r) \text{ and } r \leq 1/2; & (33b) \\[2mm] \frac{-4\Lambda^{2+2r}-4\Lambda^{2+\rho}+\Lambda^{2(r+\rho)}+4\Lambda^{2+2r+\rho}+3\Lambda^{2+2\rho}-2\Lambda^{1+r+\rho}(r+3\Lambda\rho+\Lambda^r\rho-1)\log\Lambda}{2(\Lambda^r-1)^2\rho\Lambda^{2+\rho}\log\Lambda}, \\ \qquad \text{if } \min(r, 1-r) \leq \rho \leq \max(r, 1-r) \text{ and } r \geq 1/2; & (33c) \\[2mm] \frac{-\Lambda^{2+2r}-4\Lambda^{2+\rho}+\Lambda^{2(r+\rho)}+4\Lambda^{2+2r+\rho}-2\Lambda^{1+r+\rho}(r+3\Lambda\rho+\Lambda^r\rho-1)\log\Lambda}{2(\Lambda^r-1)^2\rho\Lambda^{2+\rho}\log\Lambda}, \\ \qquad \text{if } \max(r, 1-r) \leq \rho \leq 1; & (33d) \\[2mm] \frac{2\Lambda\left(\Lambda^{2r}-1\right)-(\Lambda^r+r+3\Lambda r-1)\Lambda^r\log\Lambda}{(\Lambda^r-1)^2\rho\Lambda\log\Lambda}, \\ \qquad \text{if } \rho \geq 1. & (33e) \end{cases}$$

The proof can be found in App. B.

Propositions 1 and 2 give accurate approximations for the MAI and SI terms in the general case of PRake receivers at the access point and of exponentially decaying aPDP. Furthermore, these results confirm that the approximations are independent of large-scale fading models, as claimed in [6], since they do not depend on the variance of the users.

It is also possible to obtain results for more specific scenarios using (30) and (32) with particular values of Λ and r, as shown in the following subsections.

B. PRake with flat aPDP

The results presented above can be used to study the case of a channel model assuming flat aPDP. As already mentioned, the flat aPDP model is captured when $\Lambda = 1$. In order to obtain expressions suitable for this case, it is sufficient to let Λ go to 1 in both (30) and (32). The former yields

$$\lim_{\Lambda\to 1} \mu\left(\Lambda, r\right) = \frac{1}{r}, \tag{34}$$

while the latter gives

$$\lim_{\Lambda \to 1} \nu\left(\Lambda, r, \rho\right) = \begin{cases} \frac{2r^2 + 2r - 4\rho r + \rho^2}{2r^2}, \\ \qquad \text{if } 0 \leq \rho \leq \min(r, 1-r); & (35\text{a}) \\[2mm] \frac{1}{2}\left(\frac{2-\rho}{r} + \frac{r}{\rho} - 1\right), \\ \qquad \text{if } \min(r, 1-r) \leq \rho \leq \max(r, 1-r) \text{ and } r \leq 1/2; & (35\text{b}) \\[2mm] \frac{r^3 + r^2(9\rho - 3) + r(3 - 9\rho^2) + 4\rho^3 - 3\rho^2 + 3\rho - 1}{6\rho r^2}, \\ \qquad \text{if } \min(r, 1-r) \leq \rho \leq \max(r, 1-r) \text{ and } r \geq 1/2; & (35\text{c}) \\[2mm] \frac{4r^3 - 3r^2 + 3r + (\rho - 1)^3}{6\rho r^2}, \\ \qquad \text{if } \max(r, 1-r) \leq \rho \leq 1; & (35\text{d}) \\[2mm] \frac{4r^2 - 3r + 3}{6\rho r}, \\ \qquad \text{if } \rho \geq 1. & (35\text{e}) \end{cases}$$

C. ARake with exponentially decaying aPDP

The results of Props. 1-2 can also describe the model of a wireless network using ARake receivers at the access point. As noticed in Sect. II-A, an ARake receiver is a PRake receiver with $r = 1$. Letting r go to 1 in (30) and (32), it is possible to obtain approximations for the MAI and SI terms in a multipath channel with exponentially decaying aPDP as follows:

$$\mu_A\left(\Lambda\right) = \lim_{r \to 1} \mu\left(\Lambda, r\right) = 1, \tag{36}$$

$$\nu_A\left(\Lambda, \rho\right) = \lim_{r \to 1} \nu\left(\Lambda, r, \rho\right) = \begin{cases} \frac{2\left(\Lambda^2 - 1 + \Lambda^\rho - \Lambda^{2-\rho} - 2\Lambda\rho \log \Lambda\right)}{\left(\Lambda - 1\right)^2 \rho \log \Lambda}, & \text{if } \rho \leq 1, \\ \frac{2\left(\Lambda^2 - 1 - 2\Lambda \log \Lambda\right)}{\left(\Lambda - 1\right)^2 \rho \log \Lambda}, & \text{if } \rho \geq 1. \end{cases} \tag{37}$$

It is worth noting that the result for $\rho \leq 1$ in (37) has been obtained by letting $r \to 1$ in (33c).

D. ARake with flat aPDP

The simplest case is represented by a wireless network using the ARake receivers at the access point, where the channel is assumed to have a flat aPDP. This situation can be captured by simultaneously

letting both Λ and r go to 1 in (30) and (32). This approach gives

$$\lim_{\substack{\Lambda \to 1, \\ r \to 1}} \mu\left(\Lambda, r\right) = 1, \tag{38}$$

$$\lim_{\substack{\Lambda \to 1, \\ r \to 1}} \nu\left(\Lambda, r, \rho\right) = \begin{cases} \dfrac{2}{3}\left(\rho^2 - 3\rho + 3\right), & \text{if } \rho \le 1, \\ 2/(3\rho), & \text{if } \rho \ge 1. \end{cases} \tag{39}$$

As in (37), the result for $\rho \le 1$ in (39) has been obtained by letting $r \to 1, \Lambda \to 1$ in (33c).

It is worth noting that (38) and (39) coincide with the results obtained in [6] for the specific case of ARake receivers and flat aPDP.

E. Comments on the Results

This subsection contains some comments on the results provided by Props. 1-2, applied both to the general case of the PRake receivers with an exponentially decaying aPDP and to its subcases.

Fig. 3 shows the shape of the term $\mu\left(\Lambda, r\right)$, proportional to the MAI as in (30), versus the ratio r for some values of Λ. The solid line represents $\Lambda = 0\,\text{dB}$, while the dashed and the dotted line depict $\Lambda = 10\,\text{dB}$ and $\Lambda = 20\,\text{dB}$, respectively. As can be seen, $\mu\left(\Lambda, r\right)$ decreases as either Λ or r increases. Keeping r fixed, it makes sense that $\mu\left(\Lambda, r\right)$ is a decreasing function of Λ, since the received power of the other users is lower as Λ increases. Keeping Λ fixed, it makes sense that $\mu\left(\Lambda, r\right)$ is a decreasing function of r, since the receiver uses a higher number of coefficients, thus better mitigating the effect of MAI. Furthermore, it can be seen that, for an ARake, $\lim_{r \to 1} \mu\left(\Lambda, r\right) = \mu_A\left(\Lambda\right) = 1$ irrespectively of Λ.

Fig. 4 shows the shape of the term $\nu\left(\Lambda, r, \rho\right)$, proportional to the SI as in (32), versus the ratio r for some values of Λ and ρ. The solid line represents $\Lambda = 0\,\text{dB}$, while the dashed and the dotted line depict $\Lambda = 10\,\text{dB}$ and $\Lambda = 20\,\text{dB}$, respectively. The circles represent $\rho = 0.25$, while the square markers and the rhombi report the shape of $\nu\left(\Lambda, r, \rho\right)$ for $\rho = 1.0$ and $\rho = 4.0$, respectively. As can be verified, $\nu\left(\Lambda, r, \rho\right)$ decreases as either ρ or Λ increases. This behavior of $\nu\left(\Lambda, r, \rho\right)$ wrt ρ is justified by the higher resistance to multipath due to increasing the number of possible positions and thus the length of a single frame. This also agrees with the results of [6] and [14], where it has been shown that, for a fixed total processing gain N, systems with higher N_c outperform those with smaller N_c, due to higher mitigation of SI. Similarly to $\mu\left(\Lambda, r\right)$, it makes sense that $\nu\left(\Lambda, r, \rho\right)$ is a decreasing function of Λ when r and ρ are fixed, since the neglected paths are weaker as Λ increases. Taking into account the behavior of $\nu\left(\Lambda, r, \rho\right)$ as a function of r, it can be verified, either analytically or graphically, that $\nu\left(\Lambda, r, \rho\right)$ is not monotonically decreasing as r increases. In other words, an ARake receiver using MRC does not offer the

optimum performance in mitigating the effect of SI, but it is outperformed by the PRake receivers whose r decreases as Λ increases. This behavior is due to the fact that the receiver uses MRC, which attempts to gather all the signal energy to maximize the signal-to-noise ratio (SNR) and substantially ignores the effects of SI [22]. In this scenario, a minimum mean square error (MMSE) combining criterion [23], while more complex, might give a different comparison.

IV. ANALYSIS OF THE NASH EQUILIBRIUM

Making use of the analysis presented in the previous section, it is possible to study the performance of the PRake receivers in terms of achieved utilities when the noncooperative power control techniques described in Sect. II-B are adopted.

A. Analytical Results

Using Props. 1 and 2 in (11) and (15), it is straightforward to obtain the expressions for transmit powers p_k^* and utilities u_k^* achieved at the Nash equilibrium, which are independent of the channel realizations of the other users, and of SI:

$$p_k^* \overset{a.s.}{\to} \frac{1}{h_k^{(\text{SP})}} \cdot \frac{N\sigma^2 \Gamma\left(\frac{N}{\nu(\Lambda,r,\rho)}\right)}{N - \Gamma\left(\frac{N}{\nu(\Lambda,r,\rho)}\right) \cdot \left[(K-1)\mu\left(\Lambda,r\right) + \nu\left(\Lambda,r,\rho\right)\right]}, \tag{40}$$

$$u_k^* \overset{a.s.}{\to} h_k^{(\text{SP})} \cdot \frac{D}{M} R_k \cdot f\left(\Gamma\left(\frac{N}{\nu\left(\Lambda,r,\rho\right)}\right)\right) \cdot \frac{N - \Gamma\left(\frac{N}{\nu(\Lambda,r,\rho)}\right) \cdot \left[(K-1)\mu\left(\Lambda,r\right) + \nu\left(\Lambda,r,\rho\right)\right]}{N\sigma^2 \Gamma\left(\frac{N}{\nu(\Lambda,r,\rho)}\right)}. \tag{41}$$

Note that (40)-(41) require knowledge of the channel realization for user k (through $h_k^{(\text{SP})}$).

Analogously, (16) translates into the system design parameter

$$N_f \geq \left\lceil \Gamma\left(\frac{N}{\nu\left(\Lambda,r,\rho\right)}\right) \cdot \frac{(K-1)\mu\left(\Lambda,r\right) + \nu\left(\Lambda,r,\rho\right)}{N_c} \right\rceil, \tag{42}$$

where $\lceil\cdot\rceil$ is the ceiling operator.

Prop. 3: In the asymptotic case where the hypotheses of Theorem 1 hold, the loss Ψ of a PRake receiver wrt an ARake receiver in terms of achieved utilities converges a.s. to

$$\Psi = \frac{u_{k_A}^*}{u_k^*} \overset{a.s.}{\to} \mu\left(\Lambda,r\right) \cdot \frac{f\left(\Gamma\left(\frac{N}{\nu_A(\Lambda,\rho)}\right)\right)}{f\left(\Gamma\left(\frac{N}{\nu(\Lambda,r,\rho)}\right)\right)} \cdot \frac{\Gamma\left(\frac{N}{\nu(\Lambda,r,\rho)}\right)}{\Gamma\left(\frac{N}{\nu_A(\Lambda,\rho)}\right)} \cdot \frac{N - \Gamma\left(\frac{N}{\nu_A(\Lambda,\rho)}\right)\left[(K-1)\mu_A\left(\Lambda\right) + \nu_A\left(\Lambda,\rho\right)\right]}{N - \Gamma\left(\frac{N}{\nu(\Lambda,r,\rho)}\right)\left[(K-1)\mu\left(\Lambda,r\right) + \nu\left(\Lambda,r,\rho\right)\right]}, \tag{43}$$

where $u_{k_A}^*$ is the utility achieved by an ARake receiver.

The proof can be found in App. C.

Equation (43) also provides a system design criterion. Given L, N_c, N_f, K and Λ, a desired loss Ψ can in fact be achieved using the ratio r obtained by numerically inverting (43). Unlike (40)-(41), this result is independent of all channel realizations.

B. Simulation Results

In this subsection, we show numerical results for the analysis presented in the previous subsection. Simulations are performed using the iterative algorithm described in detail in [6]. The systems we examine have the design parameters listed in Table I. We use the efficiency function $f(\gamma_k) = (1 - e^{-\gamma_k/2})^M$ as a reasonable approximation to the PSR [4], [14]. To model the UWB scenario, the channel gains are assumed as in Sect. III, with $\sigma_k^2 = 0.3 d_k^{-2}$, where d_k is the distance between the kth user and the access point. Distances are assumed to be uniformly distributed between 3 and $20\,\text{m}$.

Fig. 5 shows the probability P_o of having at least one user transmitting at the maximum power, i.e., $P_o = \Pr\{\max_k p_k = \overline{p} = 1\,\mu\text{W}\}$, as a function of the number of frames N_f. We consider $10\,000$ realizations of the channel gains, using a network with $K = 8$ users, $N_c = 50$, $L = 200$ (thus $\rho = 0.25$), and PRake receivers with $L_P = 20$ coefficients (and thus $r = 0.1$). The solid line represents the case $\Lambda = 0\,\text{dB}$, while the dashed and the dotted lines depict the cases $\Lambda = 10\,\text{dB}$ and $\Lambda = 20\,\text{dB}$, respectively. Note that the slope of P_o increases as Λ increases. This phenomenon is due to reducing the effects of neglected path gains as Λ becomes higher, which, given N_f, results in having more homogeneous effects of neglected gains. Using the parameters above in (42), the minimum value of N_f that allows all K users to simultaneously achieve the optimum SINRs is $N_f = \{21, 9, 6\}$ for $\Lambda = \{0\,\text{dB}, 10\,\text{dB}, 20\,\text{dB}\}$, respectively. As can be seen, the analytical results closely match those from simulations. It is worth emphasizing that (42) is valid for both L and L_P going to ∞, as stated in Props. 1-2. In this example, $L_P = 20$, which does not fulfill this hypothesis. This explains the slight mismatch between theoretical and simulation results, especially for small Λ's. However, showing numerical results for a feasible system is more interesting than simulating a network with a very high number of PRake coefficients.

Fig. 6 shows a comparison between analytical and numerical achieved utilities as a function of the channel gains $h_k = ||\boldsymbol{\alpha}_k||^2$. The network has the following parameters: $K = 8$, $L = 200$, $N_c = 50$, $N_f = 20$, $\Lambda = 10\,\text{dB}$, $\rho = 0.25$. The markers correspond to the simulation results given by a single realization of the path gains. Some values of the number of coefficients of the PRake receiver are considered. In particular, the square markers report the results for the ARake ($r = 1$), while triangles, circles and rhombi show the cases $r = \{0.5, 0.3, 0.1\}$, respectively. The solid line represents the theoretical achieved utility, computed using (41). The dashed, the dash-dotted and the dotted lines have been obtained by subtracting

from (41) the loss Ψ, computed as in (43). Using the parameters above, $\Psi = \{1.34\,\mathrm{dB}, 2.94\,\mathrm{dB}, 8.40\,\mathrm{dB}\}$ for $r = \{0.5, 0.3, 0.1\}$, respectively. As before, the larger the number of L_P coefficients is, the smaller the difference between theoretical analysis and simulations is. It is worth noting that the theoretical results do not consider the actual values of $h_k^{(\mathrm{SP})}$, as required in (41),[4] since they make use of the asymptotic approximation (43). As can be verified, the analytical results closely match the actual performance of the PRake receivers, especially recalling that the results are not averaged. Only a single random channel realization is in fact considered, because we want to emphasize that not only this approximation is accurate on average, but also that the normalized mean square error (nmse) $\mathrm{nmse}\,(u_k^*) = \mathbb{E}\{[(u_{k_A}^*/\Psi - u_k^*)/u_k^*]^2\}$ is considerably low, where $\mathbb{E}\{\cdot\}$ denotes expectation; $u_{k_A}^*$ and Ψ are *computed* following (41) and (43), respectively; and u_k^* represents the *experimental* utility at the Nash equilibrium. In fact, by averaging over $10\,000$ channel realizations using the same network parameters, $\mathrm{nmse}\,(u_k^*) = \{1.4 \times 10^{-3}, 5.9 \times 10^{-3}, 6.3 \times 10^{-2}\}$ for $r = \{0.5, 0.3, 0.1\}$, respectively, As a conclusion, this allows every network fulfilling the above described hypotheses to be studied with the proposed tools.

Fig. 7 shows the loss Ψ versus the ratio r for some values of Λ and ρ. The network parameters are set as follows: $K = 8$, $N_f = 20$, and $L = 200$. The solid lines represent $\Lambda = 0\,\mathrm{dB}$, while the dashed lines depict $\Lambda = 10\,\mathrm{dB}$. The circles represent $N_c = 50$ (and thus $\rho = 0.25$), while the square markers report $N_c = 200$ (and thus $\rho = 1.0$). As is obvious, Ψ is a decreasing function of r. Furthermore, Ψ is a decreasing function of Λ, since the received power associated to the paths neglected by the PRake receiver is lower as Λ increases. Similarly, keeping the number of multiple paths L fixed, Ψ decreases as ρ increases. This complies with theory [6], [14], since increasing the processing gain provides higher robustness against multipath. As a consequence, a system with a lower ρ benefits more from a higher number of fingers at the receiver than a system with a higher ρ does. Hence, when ρ is lower, a PRake receiver performs worse, i.e., Ψ is higher.

It is worth stating that the proposed analysis is mainly focused on energy efficiency. Hence, the main performance index here is represented by the achieved utility at the Nash equilibrium. However, more traditional measures of performance such as SINR or bit error rate (BER) can be obtained using the parameters derived here. In fact, typical target SINRs at the access point can be computed using $\gamma_k^* = \Gamma\left(N/\nu\left(\Lambda, r, \rho\right)\right)$, as derived in the previous sections. Similarly, the BER can be approximated by $Q\left(\sqrt{\gamma_k^*}\right)$ [14], where $Q(\cdot)$ denotes the complementary cumulative distribution function of a standard normal random variable.

---

[4]This is also valid for the case ARake, since $h_k^{(\mathrm{SP})} = h_k$.

V. CONCLUSION

In this paper, we have a used a large-system analysis to study performance of PRake receivers using maximal ratio combining when energy-efficient power control techniques are adopted. We have considered a wireless data network in frequency-selective environments, where the user terminals transmit IR-UWB signals to a common concentration point. Assuming the averaged power delay profile and the amplitude of the path coefficients to be exponentially decaying and Rayleigh-distributed, respectively, we have obtained a general characterization for the terms due to multiple access interference and self-interference. The expressions are dependent only on the network parameters and the number of PRake coefficients. A measure of the loss of the PRake receivers with respect to the ARake receiver has then been proposed which is completely independent of the channel realizations. This theoretical approach may also serve as a criterion for network design, since it is completely described by the network parameters.

APPENDIX

A. Proof of Prop. 1

To derive (30), we make use of the result (17) of Theorem 1. Using the hypotheses shown in Sect. III, $\mathbf{D}_k^\alpha$ and $\mathbf{D}_k^\beta$ are represented by (27) and (28), respectively.

Hence, focusing on the denominator of (17),

$$\varphi\left(\mathbf{D}_k^\alpha\mathbf{D}_k^\beta\right) = \lim_{L\to\infty}\frac{1}{L}\sum_{l=1}^{L}\{\mathbf{D}_k^\alpha\mathbf{D}_k^\beta\}_l = \lim_{L\to\infty}\frac{\sigma_k^2}{L}\sum_{l=1}^{rL}\Lambda^{-\frac{l-1}{L-1}} = \sigma_k^2\cdot\frac{\Lambda^r-1}{\Lambda^r\log\Lambda}. \tag{44}$$

Analogously,

$$\varphi\left(\mathbf{D}_j^\alpha\mathbf{D}_j^\beta\right) = \sigma_j^2\cdot\frac{\Lambda^r-1}{\Lambda^r\log\Lambda}. \tag{45}$$

Using (7), (8) and (25), after some algebraic manipulation, we obtain

$$\{\mathbf{C}_j^\alpha\mathbf{C}_j^{\alpha H}\}_{ll} = \frac{\sigma_j^2}{L}\left(\sum_{m=l+1}^{L}\Lambda^{-\frac{m-1}{L-1}}\right)u\left[L-1-l\right], \tag{46}$$

$$\{\mathbf{C}_k^\beta\mathbf{C}_k^{\beta H}\}_{ll} = \frac{\sigma_k^2}{L}\left(\sum_{m=l+1}^{rL}\Lambda^{-\frac{m-1}{L-1}}\right)u\left[rL-1-l\right], \tag{47}$$

where $u\left[\cdot\right]$ is defined as in (29). The terms in the numerator of (17) thus translate into

$$\varphi\left(\mathbf{D}_j^\alpha\mathbf{C}_k^\beta\mathbf{C}_k^{\beta H}\mathbf{D}_j^\alpha\right) = \lim_{L\to\infty}\frac{1}{L}\sum_{l=1}^{L}\{\mathbf{D}_j^\alpha\}_l^2\{\mathbf{C}_k^\beta\mathbf{C}_k^{\beta H}\}_{ll}$$

$$= \lim_{L\to\infty}\frac{\sigma_k^2\sigma_j^2}{L^2}\sum_{l=1}^{rL-1}\Lambda^{-\frac{l-1}{L-1}}\sum_{m=l+1}^{rL}\Lambda^{-\frac{m-1}{L-1}} = \sigma_k^2\sigma_j^2\cdot\frac{\Lambda^{-2r}\left(\Lambda^r-1\right)^2}{2\left(\log\Lambda\right)^2} \tag{48}$$

and

$$\varphi\left(\mathbf{D}_k^\beta \mathbf{C}_j^\alpha \mathbf{C}_j^{\alpha H} \mathbf{D}_k^\beta\right) = \lim_{L\to\infty} \frac{1}{L} \sum_{l=1}^L \{\mathbf{D}_k^\beta\}_l^2 \{\mathbf{C}_j^\alpha \mathbf{C}_j^{\alpha H}\}_{ll} = \lim_{L\to\infty} \frac{\sigma_k^2 \sigma_j^2}{L^2} \sum_{l=1}^{rL} \Lambda^{-\frac{l-1}{L-1}} \sum_{m=l+1}^{L} \Lambda^{-\frac{m-1}{L-1}}$$

$$= \sigma_k^2 \sigma_j^2 \cdot \frac{\Lambda^{-1-2r}\left(\Lambda^r - 1\right)\left(\Lambda - 2\Lambda^r + \Lambda^{r+1}\right)}{2\left(\log\Lambda\right)^2}. \tag{49}$$

Using (44)-(45) and (48)-(49),

$$\frac{h_{kj}^{(\text{MAI})}}{h_j^{(\text{SP})}} \xrightarrow{a.s.} \frac{1}{N} \cdot \frac{\varphi\left(\mathbf{D}_j^\alpha \mathbf{C}_k^\beta \mathbf{C}_k^{\beta H} \mathbf{D}_j^\alpha\right) + \varphi\left(\mathbf{D}_k^\beta \mathbf{C}_j^\alpha \mathbf{C}_j^{\alpha H} \mathbf{D}_k^\beta\right)}{\varphi\left(\mathbf{D}_j^\alpha \mathbf{D}_j^\beta\right) \cdot \varphi\left(\mathbf{D}_k^\alpha \mathbf{D}_k^\beta\right)} = \frac{1}{N} \cdot \frac{\left(\Lambda - 1\right)\Lambda^{r-1}}{\Lambda^r - 1}. \tag{50}$$

Using (50), the result (30) is straightforward.

B. Proof of Prop. 2

To derive (32), we make use of the result (18) of Theorem 1. Using the hypotheses shown in Sect. III, $\mathbf{D}_k^\alpha$ and $\mathbf{D}_k^\beta$ are represented by (27) and (28), respectively. The denominator can be obtained following the same steps as in App. A:

$$\left(\varphi\left(\mathbf{D}_k^\alpha \mathbf{D}_k^\beta\right)\right)^2 = \sigma_k^4 \cdot \frac{\left(\Lambda^r - 1\right)^2}{\Lambda^{2r}\left(\log\Lambda\right)^2}. \tag{51}$$

Following (24),

$$\theta_k^2\left(l, L + l - i\right) = \sigma_k^4 \cdot \Lambda^{-\frac{L+2l-i-2}{L-1}} \cdot w\left[l, i\right], \tag{52}$$

where

$$w\left[l, i\right] = u\left[rL - l\right] + u\left[rL - L + i - l\right]$$
$$+ 2u\left[rL - l\right] \cdot u\left[rL - L + i - l\right] \tag{53}$$

has been introduced for convenience of notation.

In order to obtain explicit expressions for $w\left[l, i\right]$, it is convenient to split the range of r into the two following cases.

- $r \le 1/2$: taking into account all the possible values of l and i,

$$w\left[l, i\right] = \begin{cases} 4, & \text{if } L - rL + 1 \le i \le L - 1 \text{ and } 1 \le l \le rL - L + i; \\ 1, & \text{either if } 1 \le i \le rL \text{ and } 1 \le l \le 1, \\ & \text{or if } rL \le i \le L - rL \text{ and } 1 \le l \le rL, \\ & \text{or if } L - rL + 1 \le i \le L - 1 \text{ and } rL - L + i + 1 \le l \le rL; \\ 0, & \text{elsewhere.} \end{cases} \tag{54}$$

Substituting (24) and (54) in the numerator of (18) yields

$$\frac{1}{\sigma_k^4} \sum_{i=1}^{L-1} \phi_i^2 \cdot \sum_{l=1}^{i} \theta_k^2 (l, L + l - i) =$$

$$= \sum_{i=1}^{rL} \phi_i^2 \cdot \sum_{l=1}^{i} \Lambda^{-\frac{L+2l-i-2}{L-1}} + \sum_{i=rL+1}^{L-rL} \phi_i^2 \cdot \sum_{l=1}^{rL} \Lambda^{-\frac{L+2l-i-2}{L-1}}$$

$$+ \sum_{i=L-rL+1}^{L-1} \phi_i^2 \cdot \sum_{l=1}^{rL-L+i} 4\Lambda^{-\frac{L+2l-i-2}{L-1}} + \sum_{i=L-rL+1}^{L-1} \phi_i^2 \cdot \sum_{l=rL-L+i+1}^{rL} \Lambda^{-\frac{L+2l-i-2}{L-1}}; \tag{55}$$

- $r \geq 1/2$: taking into account all the possible values of l and i,

$$w[l, i] = \begin{cases} 4, & \text{either if } L - rL + 1 \leq i \leq rL \text{ and } 1 \leq l \leq rL - L + i, \\ & \text{or if } rL + 1 \leq i \leq L - 1 \text{ and } 1 \leq l \leq rL - L + i; \\ 1, & \text{either if } 1 \leq i \leq L - rL \text{ and } 1 \leq l \leq 1, \\ & \text{or if } L - rL + 1 \leq i \leq rL \text{ and } rL - L + i + 1 \leq l \leq i, \\ & \text{or if } rL + 1 \leq i \leq L - 1 \text{ and } rL - L + i + 1 \leq l \leq rL; \\ 0, & \text{elsewhere.} \end{cases} \tag{56}$$

Substituting (24) and (56) in the numerator of (18) yields

$$\frac{1}{\sigma_k^4} \sum_{i=1}^{L-1} \phi_i^2 \cdot \sum_{l=1}^{i} \theta_k^2 (l, L + l - i) = \sum_{i=1}^{L-rL} \phi_i^2 \cdot \sum_{l=1}^{i} \Lambda^{-\frac{L+2l-i-2}{L-1}}$$

$$+ \sum_{i=L-rL+1}^{rL} \phi_i^2 \cdot \sum_{l=1}^{rL-L+i} 4\Lambda^{-\frac{L+2l-i-2}{L-1}} + \sum_{i=L-rL+1}^{rL} \phi_i^2 \cdot \sum_{l=rL-L+i+1}^{i} \Lambda^{-\frac{L+2l-i-2}{L-1}}$$

$$+ \sum_{i=rL+1}^{L-1} \phi_i^2 \cdot \sum_{l=1}^{rL-L+i} 4\Lambda^{-\frac{L+2l-i-2}{L-1}} + \sum_{i=rL+1}^{L-1} \phi_i^2 \cdot \sum_{l=rL-L+i+1}^{rL} \Lambda^{-\frac{L+2l-i-2}{L-1}}. \tag{57}$$

In order to obtain (33a)-(33e), the explicit values of ϕ_i^2 must be used. From (9)-(10) follows

$$\phi_i^2 = \begin{cases} (L-i)/N_c, & \text{either if } N_c \leq L \text{ and } L - N_c + 1 \leq i \leq L - 1, \\ & \text{or if } N_c \geq L \text{ and } 1 \leq i \leq L - 1; \\ 1, & \text{if } N_c \leq L \text{ and } 1 \leq i \leq L - N_c. \end{cases} \tag{58}$$

As in the case of r, it is convenient to separate the range of $\rho = N_c/L$ in the following cases.

- $0 \le \rho \le \min(r, 1-r)$: substituting (58) in (55) and (57), they both yield

$$\frac{1}{\sigma_k^4} \lim_{L\to\infty} \frac{1}{L^2} \sum_{i=1}^{L-1} \phi_i^2 \cdot \sum_{l=1}^{i} \theta_k^2 (l, L+l-i) = \frac{\Lambda\left(\Lambda^r-1\right)\left(4\Lambda^{2r}+3\Lambda^\rho-1\right)}{2\Lambda^{\rho+2r+1}\rho\left(\log\Lambda\right)^3} \\ -\frac{2\Lambda^{r+\rho}\left(\Lambda^r+3\Lambda-1\right)\rho\log\Lambda}{2\Lambda^{\rho+2r+1}\rho\left(\log\Lambda\right)^3}. \tag{59}$$

Making use of (18), (51) and (59), the results (32) and (33a) are straightforward.

- $\min(r, 1-r) \le \rho \le \max(r, 1-r)$ and $r \le 1/2$: substituting (58) in (55) yields

$$\frac{1}{\sigma_k^4} \lim_{L\to\infty} \frac{1}{L^2} \sum_{i=1}^{L-1} \phi_i^2 \cdot \sum_{l=1}^{i} \theta_k^2 (l, L+l-i) = \frac{\Lambda\left(\Lambda^{2r}-1\right)\left(4\Lambda^\rho-1\right)}{2\Lambda^{\rho+2r+1}\rho\left(\log\Lambda\right)^3} \\ -\frac{2\Lambda^{r+\rho}\left(3\Lambda r-\rho+\Lambda^r\rho\right)\log\Lambda}{2\Lambda^{\rho+2r+1}\rho\left(\log\Lambda\right)^3}. \tag{60}$$

Making use of (18), (51) and (60), the results (32) and (33b) are straightforward.

- $\min(r, 1-r) \le \rho \le \max(r, 1-r)$ and $r \ge 1/2$: substituting (58) in (57) yields

$$\frac{1}{\sigma_k^4} \lim_{L\to\infty} \frac{1}{L^2} \sum_{i=1}^{L-1} \phi_i^2 \cdot \sum_{l=1}^{i} \theta_k^2 (l, L+l-i) = \frac{-4\Lambda^{2+2r}-4\Lambda^{2+\rho}+\Lambda^{2(r+\rho)}+4\Lambda^{2+2r+\rho}}{2\Lambda^{2+2r+\rho}\rho\left(\log\Lambda\right)^3} \\ +\frac{3\Lambda^{2+2\rho}-2\rho^{\rho+r+1}\left(\Lambda^r\rho+3\Lambda\rho+r-1\right)\log\Lambda}{2\Lambda^{2+2r+\rho}\rho\left(\log\Lambda\right)^3}. \tag{61}$$

Making use of (18), (51) and (61), the results (32) and (33c) are straightforward.

- $\max(r, 1-r) \le \rho \le 1$: substituting (58) into (55) and (57), they both yield

$$\frac{1}{\sigma_k^4} \lim_{L\to\infty} \frac{1}{L^2} \sum_{i=1}^{L-1} \phi_i^2 \cdot \sum_{l=1}^{i} \theta_k^2 (l, L+l-i) = \frac{-\Lambda^{2+2r}-4\Lambda^{2+\rho}+\Lambda^{2(r+\rho)}+4\Lambda^{2+2r+\rho}}{2\Lambda^{2+2r+\rho}\rho\left(\log\Lambda\right)^3} \\ -\frac{2\rho^{\rho+r+1}\left(\Lambda^r\rho+3\Lambda\rho+r-1\right)\log\Lambda}{2\Lambda^{2+2r+\rho}\rho\left(\log\Lambda\right)^3}. \tag{62}$$

Making use of (18), (51) and (62), the results (32) and (33d) are straightforward.

- $\rho = N_c/L \ge 1$: substituting (58) into (55) and (57), they both yield

$$\frac{1}{\sigma_k^4} \lim_{L\to\infty} \frac{1}{L^2} \sum_{i=1}^{L-1} \phi_i^2 \cdot \sum_{l=1}^{i} \theta_k^2 (l, L+l-i) = \frac{2\Lambda\left(\Lambda^{2r}-1\right)-\left(\Lambda^r+r+3\Lambda r-1\right)\Lambda^r\log\Lambda}{\Lambda^{2r+1}\rho\left(\log\Lambda\right)^3}. \tag{63}$$

Making use of (18), (51) and (63), the results (32) and (33e) are straightforward.

C. Proof of Prop. 3

At the Nash equilibrium, the transmit power for user k when using an ARake receiver at the access point, $p_{k_A}^*$, can be obtained from (15):

$$p_{k_A}^* = \frac{1}{h_k} \cdot \frac{\sigma^2 \Gamma\left(\gamma_{0,k_A}\right)}{1 - \Gamma\left(\gamma_{0,k_A}\right) \cdot \left(\gamma_{0,k_A}^{-1} + \zeta_{k_A}^{-1}\right)}, \tag{64}$$

where the subscript A serves to emphasize that we are considering the case of an ARake, and where we have used the fact that $h_k^{(\text{SP})}$ is equal to the channel gain $h_k = \boldsymbol{\alpha}_k^H \cdot \boldsymbol{\alpha}_k = ||\boldsymbol{\alpha}_k||^2$. Hence, (43) becomes

$$\Psi = \frac{h_k}{h_k^{(\text{SP})}} \cdot \frac{f\left(\Gamma\left(\gamma_{0,k_A}\right)\right)}{f\left(\Gamma\left(\gamma_{0,k}\right)\right)} \cdot \frac{\Gamma\left(\gamma_{0,k}\right)}{\Gamma\left(\gamma_{0,k_A}\right)} \cdot \frac{1 - \Gamma\left(\gamma_{0,k_A}\right) \cdot \left(\gamma_{0,k_A}^{-1} + \zeta_{k_A}^{-1}\right)}{1 - \Gamma\left(\gamma_{0,k}\right) \cdot \left(\gamma_{0,k}^{-1} + \zeta_k^{-1}\right)}. \tag{65}$$

To show that Ψ converges a.s. to the non-random limit of (43), it is convenient to rewrite the ratio $h_k/h_k^{(\text{SP})}$ as

$$\frac{h_k}{h_k^{(\text{SP})}} = \frac{\frac{1}{L}\boldsymbol{\alpha}_k^H \cdot \boldsymbol{\alpha}_k}{\frac{1}{L}\boldsymbol{\beta}_k^H \cdot \boldsymbol{\alpha}_k}. \tag{66}$$

It is possible to prove [6] that

$$\frac{1}{L}\boldsymbol{\alpha}_k^H \cdot \boldsymbol{\alpha}_k \overset{a.s.}{\to} \varphi\left((\mathbf{D}_k^\alpha)^2\right) \tag{67}$$

and, analogously,

$$\frac{1}{L}\boldsymbol{\beta}_k^H \cdot \boldsymbol{\alpha}_k \overset{a.s.}{\to} \varphi\left(\mathbf{D}_k^\alpha \mathbf{D}_k^\beta\right). \tag{68}$$

Taking into account (27),

$$\varphi\left((\mathbf{D}_k^\alpha)^2\right) = \lim_{L\to\infty} \frac{\sigma_k^2}{L} \sum_{l=1}^L \Lambda^{-\frac{l-1}{L-1}}$$

$$= \sigma_k^2 \cdot \frac{\Lambda-1}{\Lambda \log \Lambda}. \tag{69}$$

Using (44), (66) and (69),

$$\frac{h_k}{h_k^{(\text{SP})}} \overset{a.s.}{\to} \mu\left(\Lambda, r\right), \tag{70}$$

where $\mu\left(\Lambda, r\right)$ is defined as in (31).

Making use of (30), (32), (36), (37) and (70), when the hypotheses of Theorem 1 hold, (65) converges a.s. to (43).

REFERENCES

[1] A. B. MacKenzie and S. B. Wicker, "Game theory in communications: Motivation, explanation, and application to power control," in *Proc. IEEE Global Telecommun. Conf.*, San Antonio, TX, 2001, pp. 821-826.

[2] D. J. Goodman and N. B. Mandayam, "Power control for wireless data," *IEEE Pers. Commun.*, Vol. 7, pp. 48-54, Apr. 2000.

[3] C. U. Saraydar, N. B. Mandayam and D. J. Goodman, "Pricing and power control in a multicell wireless data network," *IEEE J. Sel. Areas Commun.*, Vol. 19 (10), pp. 1883-1892, Oct. 2001.

[4] C. U. Saraydar, N. B. Mandayam and D. J. Goodman, "Efficient power control via pricing in wireless data networks," *IEEE Trans. Commun.*, Vol. 50 (2), pp. 291-303, Feb. 2002.

[5] F. Meshkati, H. V. Poor, S. C. Schwartz and N. B. Mandayam, "An energy-efficient approach to power control and receiver design in wireless data networks," *IEEE Trans. Commun.*, Vol. 53 (11), pp. 1885-1894, Nov. 2005.

[6] G. Bacci, M. Luise, H. V. Poor and A. M. Tulino, "Energy-efficient power control in impulse radio UWB wireless networks," preprint, Princeton University. [Online]. Available: http://arxiv.org/pdf/cs/0701017.

[7] A. F. Molisch, J. R. Foerster and M. Pendergrass, "Channel models for ultrawideband personal area networks," *IEEE Wireless Commun.*, Vol. 10 (6), pp. 14-21, Dec. 2003.

[8] J. R. Foerster *et al.*, "Channel modeling sub-committee report final," *IEEE P802.15 Working Group for Wireless Personal Area Networks (IEEE P802.15-02/490r1-SG3a)*, Tech. Rep., Feb. 2003.

[9] A. F. Molisch, "IEEE 802.15.4a channel model - final report," *IEEE 802.15 Wireless Personal Area Network Low Rate Alternative PHY Task Group 4a (TG4a),* Tech. Rep., Nov. 2004.

[10] J. G. Proakis, *Digital Communications*, 4th ed.   New York, NY, USA: McGraw-Hill, 2001.

[11] H. Hashemi, "The indoor radio propagation channel," *Proc. IEEE*, Vol. 81 (7), pp. 943-968, Jul. 1993.

[12] M. Z. Win and R. A. Scholtz, "Ultra-wide band time-hopping spread-spectrum impulse radio for wireless multi-access communications," *IEEE Trans. Commun.*, Vol. 48 (4), pp. 679-691, Apr. 2000.

[13] Y.-P. Nakache and A. F. Molisch, "Spectral shape of UWB signals influence of modulation format, multiple access scheme, and pulse shape," in *Proc. IEEE Veh. Technol. Conf.*, Jeju, Korea, 2003, pp. 2510-2514.

[14] S. Gezici, H. Kobayashi, H. V. Poor and A. F. Molisch, "Performance evaluation of impulse radio UWB systems with pulse-based polarity randomization," *IEEE Trans. Signal Process.*, Vol. 53 (7), pp. 2537-2549, Jul. 2005.

[15] U.S. Federal Communications Commission, FCC 02-48: First Report and Order.

[16] D. N. C. Tse and P. Viswanath, *Fundamentals of Wireless Communications.*   Cambridge, UK: Cambridge Univ. Press, 2005.

[17] U. G. Schuster and H. Bölcskei, "Ultrawideband channel modeling on the basis of information-theoretic criteria," *IEEE Trans. Wireless Commun.*, 2007, to appear. [Online]. Available: http://www.nari.ee.ethz.ch/commth/pubs/p/schuster-tw06.

[18] W. P. Siriwongpairat, W. Su and K. J. R. Liu, "Performance characterization of multiband UWB communication systems using Poisson cluster arriving fading paths," *IEEE J. Sel. Areas Commun.,* Vol. 24 (4), pp. 745-751, Apr. 2006.

[19] C.-C. Chong, Y. Kim and S.-S. Lee, "A modified S-V clustering channel model for the UWB indoor residential environment," in *Proc. IEEE Veh. Technol. Conf.*, Stockholm, Sweden, 2005, pp. 58-62.

[20] S. S. Ghassemzadeh, L. J. Greenstein, T. Sveinsson, A. Kavcic and V. Tarokh, "UWB delay profile models for residential and commercial indoor environments," *IEEE Trans. Veh. Technol.*, Vol. 54 (4), pp. 1235-1244, Jul. 2005.

[21] T. Q. S. Quek, M. Z. Win and D. Dardari, "UWB transmitted reference signaling schemes - part I: performance analysis," in *Proc. IEEE Int. Conf. on Ultra-Wideband,* Zurich, Switzerland, 2005, pp. 587-592.

[22] A. G. Klein, D. R. Brown III, D. L. Goeckel, C. R. Johnson, Jr., "RAKE reception for UWB communication systems with intersymbol interference," in *Proc. IEEE Workshop on Signal Processing Advances in Wireless Communications*, Rome, Italy, 2003, pp. 244-248.

[23] S. Gezici, H. Kobayashi, H. V. Poor and A. F. Molisch, "Optimal and suboptimal linear receivers for time-hopping impulse radio systems," in *Proc. Int. Workshop on Ultra Wideband Systems*, Kyoto, Japan, 2004, p. 11-15.

TABLE I

LIST OF PARAMETERS USED IN THE SIMULATIONS.

M, total number of bits per packet	100 b
D, number of information bits per packet	100 b
R, bit rate	100 kb/s
σ^2, AWGN power at the receiver	5×10^{-16} W
$\overline{p}$, maximum power constraint	$1\,\mu$W
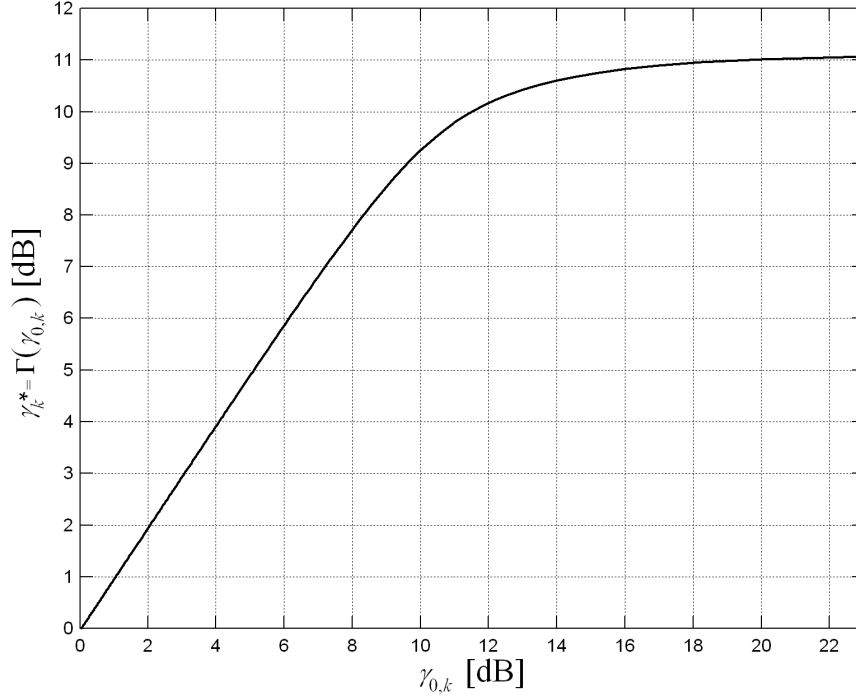
Fig. 1. Shape of γ_k^* as a function of $\gamma_{0,k}$ ($M = 100$).
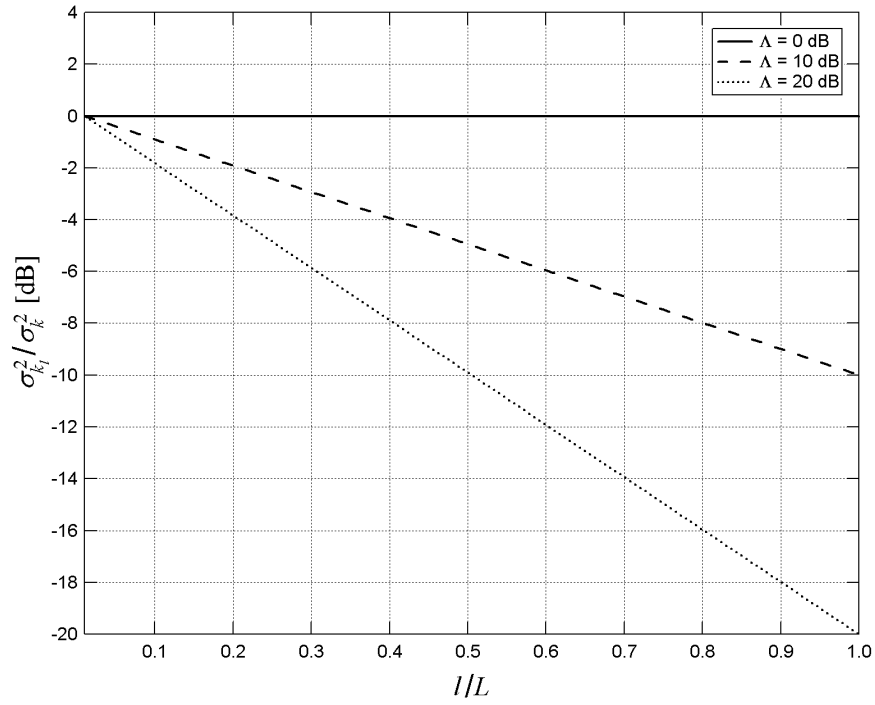
Fig. 2.   Average power delay profile versus normalized excess delay.
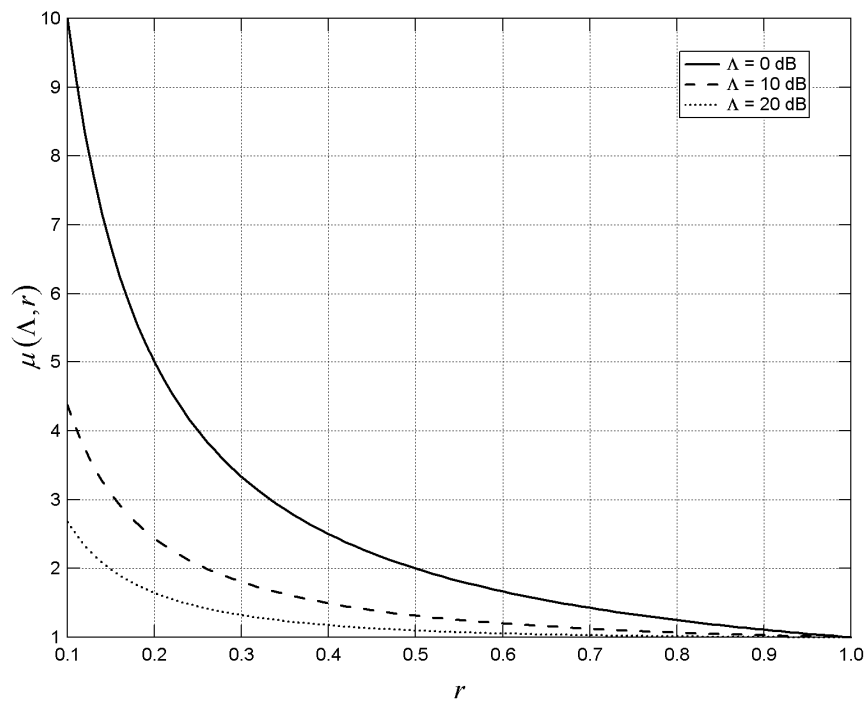
Fig. 3.   Shape of $\mu(\Lambda, r)$ versus r for some values of Λ.
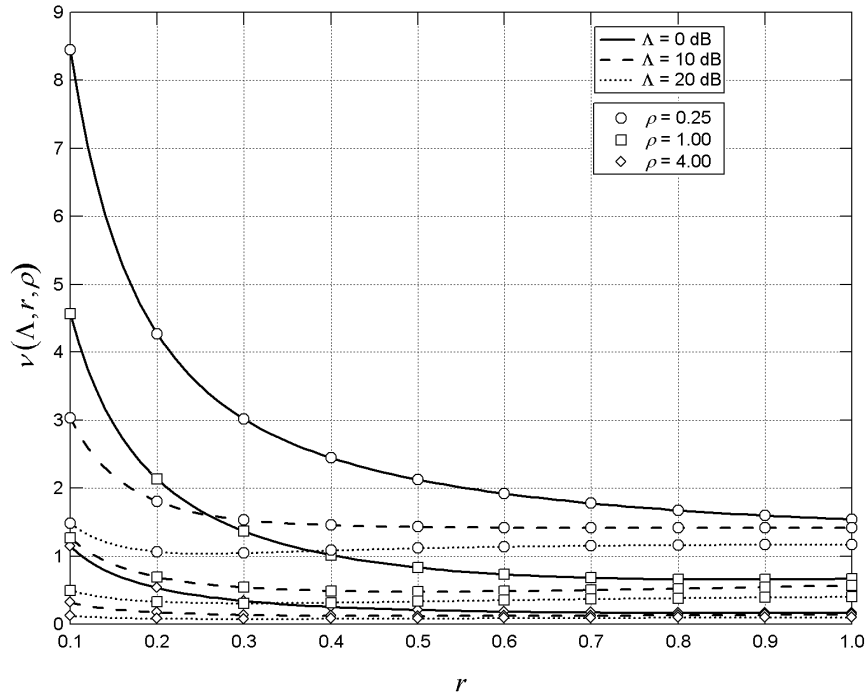
Fig. 4.   Shape of $\nu\left(\Lambda, r, \rho\right)$ versus r for some values of Λ and ρ.
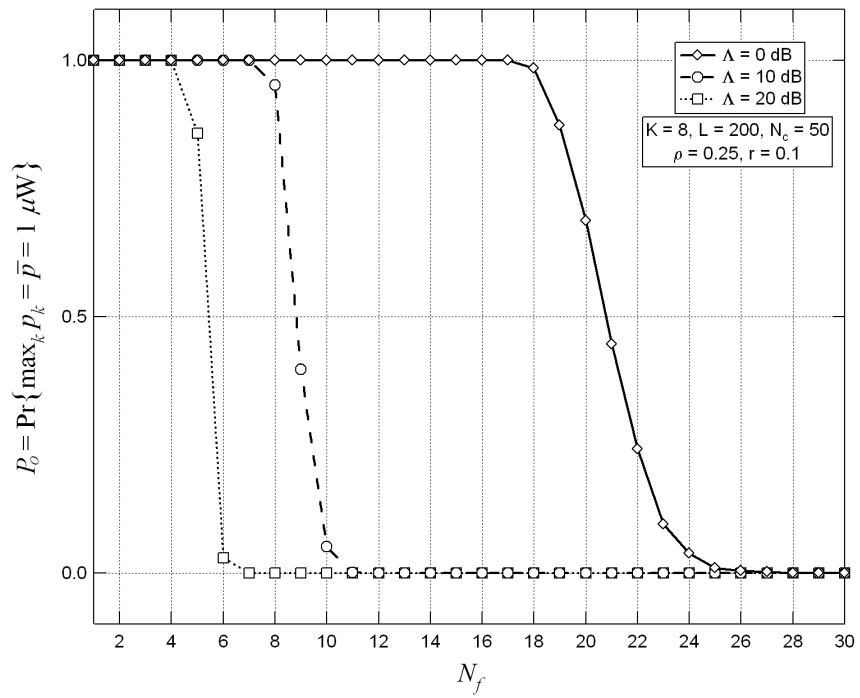
Fig. 5.   Probability of having at least one user transmitting at maximum power versus number of frames.
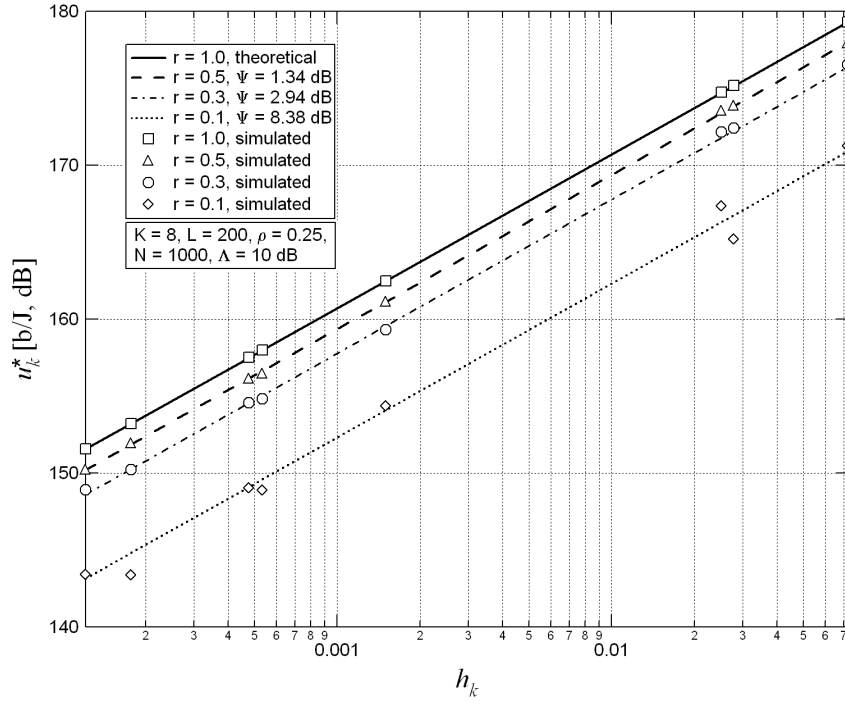
Fig. 6.   Achieved utility versus channel gain at the Nash equilibrium for different ratios r.

Fig. 7.   Shape of the loss Ψ versus the ratio r for some values of Λ and ρ.